Effect of temperature on the mechanical behaviour of an oxide/oxide composite

Antoine Débarre, Aurélie Julian-Jankowiak, Michel Parlier, Yves Renollet, Guillaume Pujol, Michel Boussuge

Effect of temperature on the mechanical behaviour of an oxide/oxide composite

A. Débarre [1,2], A. Julian-Jankowiak [1], M. Parlier [1], Y. Renollet [1], G. Pujol [3], M. Boussuge [2]

[1]*DMAS, ONERA, Université Paris-Saclay, F-92320 Châtillon*

[2] *Centre des Matériaux, MINES ParisTech, 63-65 Rue Henri Auguste Desbruères, 91100 Corbeil-Essonnes*

[3]*DGA Techniques aéronautiques, Matériaux et Technologies Plates-formes et Propulsion, 47 rue Saint-Jean, BP 93123, 31131 Balma Cedex*

Abstract: Oxide/oxide composites are being considered in the aerospace industry for the design of next-generation exhaust components. This study aims to determine the mechanical behaviour of a composite consisting in Nextel™ 610 fibres fabric (8 HSW) embedded in a porous alumina matrix. The mechanical properties were studied in tension and four-point bending up to 1300 °C. Up to 800 °C, the material behaviour is elastic and exhibits a few damage with only a low effect of the temperature. Increasing the temperature leads to the progressive apparition of a viscous behaviour up to 1000 °C and a superplastic behaviour beyond 1200 °C.

Keywords: Ceramic Matrix Composite; Oxide/Oxide; Alumina fibres; High temperature mechanical properties; Scanning Electron Microscopy

1. Introduction

The increasing demand of higher thrust-to-weight ratio requires an increase in service temperatures for high performance aero-engines. Therefore, the development of new materials able to increase the performances of engines and propulsion systems (increased efficiency, reduced pollutant emissions…) is required. Compared with metallic parts currently in use, Ceramic Matrix Composites (CMC) would allow the operating temperatures to be increased, while reducing the weight.

C and SiC fibre-reinforced ceramics offer the highest specific strength at temperature above 900 °C but also have a poor oxidation resistance at intermediate temperatures [1]–[3]. Then, for applications between 700 °C and 1000 °C in oxidising environment, oxide/oxide CMCs are investigated. Those composites, reinforced by oxide fibre fabrics, combine the fracture energy of CMCs with an inherent oxidation resistance [4]. Unlike C/C or SiC/SiC composites, a protection of the fibres against oxidizing environment is not necessary. It is therefore possible to consider composites based on the weak porous matrix principle rather than the weak interphase one [4]–[6]. That is the reason why a nanoporous matrix is considered. The porosity promotes crack deflection at the fibre/matrix interface. Oxide CMCs are also considered as lower cost materials compared to other CMCs because oxide fibers and processing without interphase are less expensive.

The mechanical behaviour of this kind of material was extensively studied at room temperature [7]–[12]. Most of the papers deal with N610 and N720 fabrics (3M Nextel) with pure alumina or aluminosilicate matrix. It was established that the mechanical behaviour is controlled by the behaviour of the fibres. The use of different kind of oxide fibres or fabrics and different processes inducing a large range of fibre volume fraction makes the comparison of the materials difficult. In particular a wide range of Young's moduli and tensile strengths (125 to 366 MPa) can be observed. Moreover, it can be noted that the strength [13] and the creep rate of the commercial fibres [13]–[17] have been improved over the years and this is difficult to take into account.

The high temperature mechanical behaviour of oxide CMCs has mainly been studied on composites with N720-based fibres under various conditions of stress, temperature and environment (water vapour) [18]–[22]. Concerning N610-based fibres composites, less studies have been conducted [23]–[25]. However, the authors mainly focused on temperatures beyond 1000 °C but did not consider the lower temperature range in which these materials are expected to operate. Only one study concerning a Nextel^{TM}610/SiO_2 composite presented some mechanical tests carried out up to 1000 °C and showed a reduction in strength of around 7% [26].

Moreover, few papers deal with damage mechanisms in this kind of materials. Damage initiation and propagation was demonstrated using micromechanical tensile tests and acoustic emission in a previous paper [12] and confirmed by other authors [27]. After the study of the tensile damage carried out by Ben Ramdane [12], we propose here to identify the damage mechanisms occurring during four-point bending tests which are more representative of the mechanical load in operating conditions. Then, the effect of the temperature on the mechanical properties is studied with tensile tests. A particular attention is paid to determine the transition temperature after which creep strain is no more negligible. Thus, a focus on the transition between the elastic and damaging domain and the viscous one is proposed.

The present work aims to understand the mechanical behaviour and the damage mechanisms of an oxide CMC at high temperatures. First, damage mechanisms at room temperature are studied through *in-situ* micromechanical bending tests in a scanning electron microscope to improve our understanding on the crack initiation and propagation under asymmetric mechanical loadings. Then, tensile and four-point bending tests from room temperature to 1300 °C, allowed three temperature domains to be identified.

2. Materials and experiments

2.1. Processing and control

The material is composed of an 8 harness satin woven fabric (similar in the 0° and 90° directions) of 3M Nextel^{TM}610 alumina fibres, desized in air at 700 °C and embedded in an alumina matrix. The fabric was infiltrated with a water-based alumina slurry and then dried [12]. A lay-up process was used to manufacture the plates: twelve layers of dried prepregs were infiltrated with controlled amount of water, piled-up in the same direction in a mould and pressed at 100 °C and low pressure in a vacuum bag. After demoulding, the plates were heat treated at 1200 °C for a few minutes to finally obtain 2.3 mm thick plates. The as-processed material is composed of 50 vol. % of fibres and around 50 vol. % of porous matrix. The total open porosity measured by the Archimedes' method is about 25 vol. % for each plate. The material has a geometrical unit cell of 8 mm x 8 mm corresponding to the weaving of the fabric.

The microstructure of the material was detailed in [12] and is shortly described here. Scanning Electron Microscopy (SEM) examinations were performed on a polished cross sections impregnated with an epoxy resin (Zeiss Gemini FEG-SEM). At low magnification (Figure 1 (a)), macropores can be observed (mainly located between plies), as well as matrix cracks perpendicular to fabric layers, created by the shrinkage of the matrix. At higher magnification (Figure 1 (b)), a nanoporosity network can be observed within the matrix.

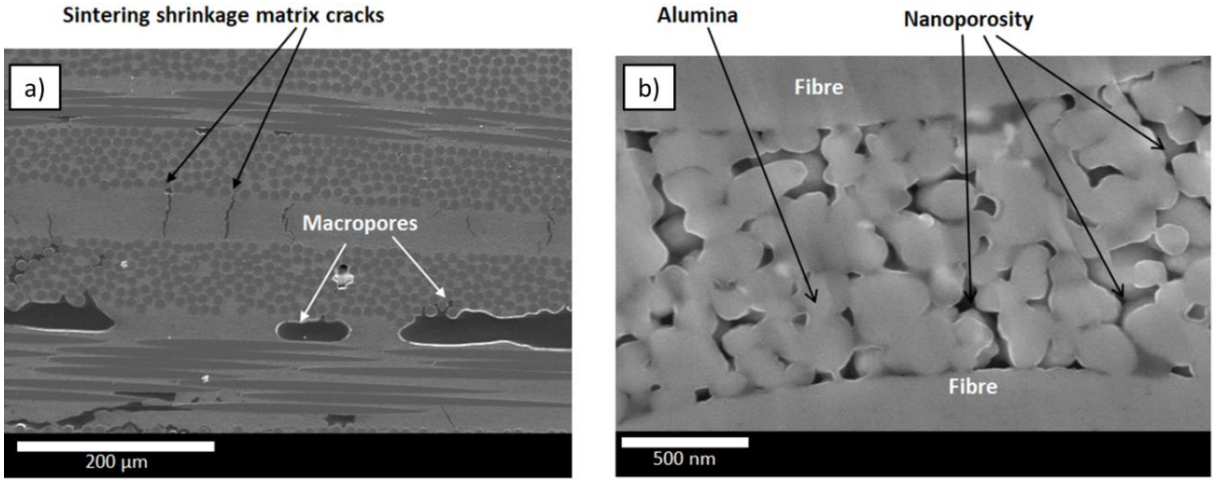

Figure 1 – SEM observation of N610/Alumina composite: matrix cracks induced by shrinkage, macropores (a) and nanoporous network (b).

The quality of each manufactured plate was verified using Non Destructive Tests (NDT). Delaminations were detected using these techniques, especially at the edges of the plates. Defective areas were eliminated when machining the specimens. It is worth noting that the macropores observed by microscopy were unfortunately too small to be detected by these methods. The shrinkage induced by sintering and the average linear Coefficient of Thermal Expansion (CTE) were determined using a high-temperature dilatometer (SETARAM, SETSYS Evolution). Experiments were conducted in air flow (30 $L.min^{-1}$) with a heating ramp of 5 $°C.min^{-1}$.

2.2. Mechanical testing

The mechanical behaviour was studied through tensile and four-point bending tests. The experimental procedures are described below and all specimen dimensions are specified in the Table 1.

In plane mechanical properties were studied through uniaxial monotonic and cyclic loadings in the fill direction. Tensile tests were carried out from room temperature to 1300 °C in air using a MTS ceramic test system with cold grips. Straight-sided specimens with a useful length of 110 mm and a widness of 16 mm were used. Depending on the temperature, the measured temperature gradient ranges between 10 to 20 °C along the gauge length of the extensometer (25 mm). After heating the samples at 400 $°C.h^{-1}$ up to the test temperature and holding them during 1 hour, tests were performed at grip displacement rates of 0.5 $mm.min^{-1}$ and 5 $µm.min^{-1}$.

For cyclic loading tests, specimens were successively loaded up to increasing stresses, with a return to null load between cycles. The stress increment between two successive cycles was 27 MPa, i.e. about 10% of the room temperature strength.

Young's moduli and damage threshold were determined graphically from stress-strain curves. The evolution of the Young's modulus was assessed on the unloading parts of cyclic tests.

Four-point bending tests were conducted from room temperature to 1050 °C in air, using a Zwick Z010 testing machine equipped with a 1 kN force cell and with outer and inner spans of respectively 40 and 20 mm. Straight sided specimen of 50 mm x 9 mm x *composite thickness* were used. At room temperature, the deflection of the centre of the specimen was measured using a LVDT sensor. At high temperature, the relative displacement of the loading points was monitored using SiC rods acting on a LVDT sensor.

Finally, *in-situ* micromechanical tests were carried out with a DEBEN MICROTEST 2kN stage at room temperature. The micromechanical setup allows tensile, compression and bending tests to be performed. The technique requires the use of specimens that are small when compared to the geometrical unit cell of the composite. Tests were carried out in a SEM (Zeiss Gemini FEG-SEM), in order to observe damage initiation and extension. In order to improve the SEM examinations, the edges of the specimens were mirror polished prior to testing, without resin impregnation. Images were acquired with a maximum imaging time of one hour while the specimens were maintained under constant displacement. The selected imaging conditions were the following: the size of the images was 10000x10000 pixels with a pixel size of 50 nm. This resolution led to the expectation that local displacement and strain fields could be measured. However, the noise-induced displacements in the images were of the same order of magnitude as those induced by the mechanical loading. Then, only damage was observed during tests under the SEM and strain field measurements were performed on the same set-up but using an optical camera. In this case, the natural texture of the material is sufficient to perform the correlation. In particular, the average strain was measured on the external plies.

	Length (mm)	Width (mm)	Thickness (mm)
Tensile Tests	200	16	composite thickness
Four-point bending tests	50	9	composite thickness
***In situ* four-point bending tests**	40	5	composite thickness

Table 1 – Dimensions of the tested N610/Alumina composite samples.

3. Results and discussion

3.1. Room temperature behaviour

3.1.1. Tensile behaviour

Representative tensile stress-strain curve recorded at room temperature is presented in Figure 2. The obtained result is in line with what was shown in the previous study [12]. The mechanical properties were measured on 12 samples issued from 3 different plates. The average tensile stress and strain at failure are 257 ± 13 MPa and 0.26 ± 0.02%. The average Young's modulus measured on the 12 samples is 159 ± 7 GPa. It has to be considered that no softening was observed, the failure occurred at the maximum stress for each tests. After this event, some fibres in the direction of loading remained intact but the material lost most of its mechanical strength.

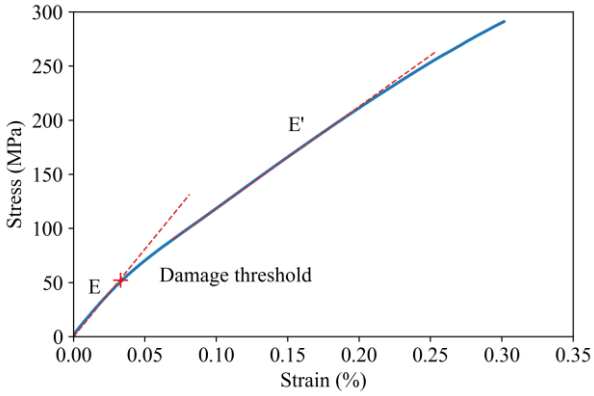

Figure 2 – Stress-strain curves in tension at room temperature of N610/alumina composite.

A knee corresponding to a loss of rigidity was systematically noticed around 50 MPa: it was identified as the damage threshold in [12] and attributed to the multi-craking of the matrix. The average stress

and strain at the damage thresholds deduced from the tensile curves are 45 ± 6 MPa and 0.029 ± 0.005% respectively.

Moreover, from the cyclic loading tests performed on 4 specimens (Figure 3 (a)) a small residual strain appearing beyond the damage threshold is observed. Small hysteresis loops can also be observed. They are generally attributed to the energy dissipated by friction between fibres and matrix. The low energy dissipation leads to a quasi-linear stress-strain curve at discharge. The stiffnesses measured on the unloading part of the curves decrease rapidly after the damage threshold and tend to 110 GPa just before failure (Figure 3 (b)). This clearly indicates a damage-effect in the matrix that occurred in the second quasi-linear domain of the stress-strain curve. This progressive damage was observed in [12] using micromechanical tests in a SEM.

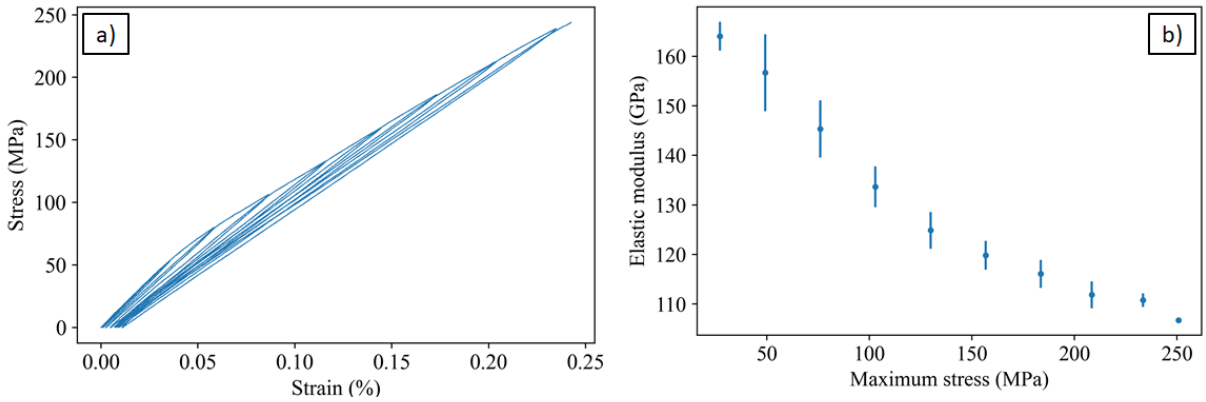

Figure 3 – Cyclic tensile loading stress-strain curve at room temperature of N610/alumina composite (a) and elastic modulus during unloading versus maximum imposed stress (b).

3.1.2. Four-point bending behaviour

The four-point bending behaviour of the material was assessed on 37 samples. Figure 4 illustrates the typical behaviour observed until the first drop in load. The bending behaviour is different from the tensile one. A change in slope was not observed, the behaviour remaining quasi-linear until failure. Solely, a progressive small deviation from linearity appeared beyond 150 MPa. The average stress and strain at failure are respectively 286 ± 52 MPa and 0.26 ± 0.05% and the elasticity modulus is 111 ± 9 GPa.

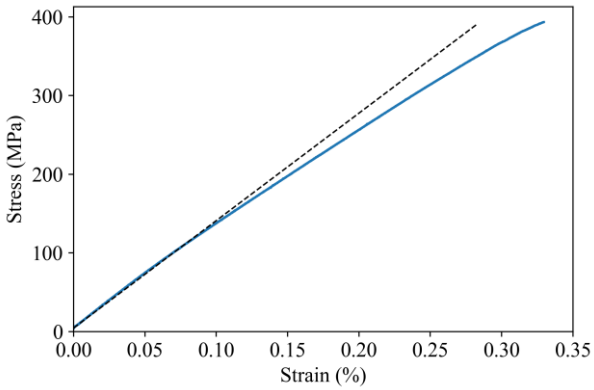

Figure 4 – Stress-strain curves in four-point bending at room temperature of N610/alumina composite.

Ben Ramdane *et al.* [12] showed that the compression behaviour can be considered as linear elastic until 200 MPa. Then, compared to tensile tests, the smaller part that progressively endures damage explains the more progressive deviation to linearity.

It is commonly accepted that the bending behaviour of SiC/SiC CMCs is dependent on the tensile behaviour because the compressive strength is much higher than the tensile one [28], [29] which is not the case for these composites. In addition, the low matrix strength makes the material sensitive to in-plane shear generated in four-point bending tests. These weaknesses combined with the presence of randomly distributed defects in the material have led to different fracture surfaces: It was reported that for 65% of the samples the failure occurred in the external plie submitted to the maximum tension. The other failures were linked to a delamination in the centre of the specimen (28%) and buckling of the ply subjected to the maximum compression stress (7%).

3.1.3. Damage observation

Strain maps were determined on images acquired with an optical camera. Average strain is calculated on a long and thin region (thickness of a ply) close to the surface as highlighted in Figure 5 (a). In tension, a progressive loss of stiffness is observed (Figure 5 (b)), which was attributed to damage and more particularly to matrix multi-cracking. The knee in the strain-stress curve is less pronounced than that observed during tensile tests. This was attributed to a partial transfer of the load to the neighbour, less-stressed ply. The curve recorded on the compressed side is linear, which is consistent with the quasi-linear elastic behaviour observed during compression tests.

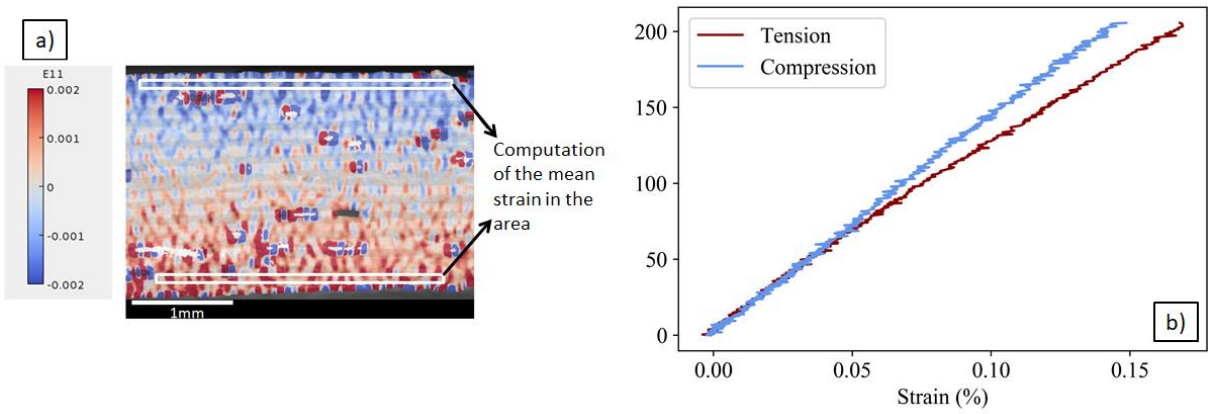

Figure 5 – Strain computation during four-point bending test on N610/alumina composite with the micromechanical setup (a) and tensile and compression stress-strain curve extraction (b).

From *in-situ* bending tests carried out in a SEM, displacement fields were determined using Digital Image Correlation. Initiations and propagations of cracks were highlighted by the presence of non-correlated areas in the displacement field as represented in Figure 6 (a). The cracks openings range from 30 to 80 nm.

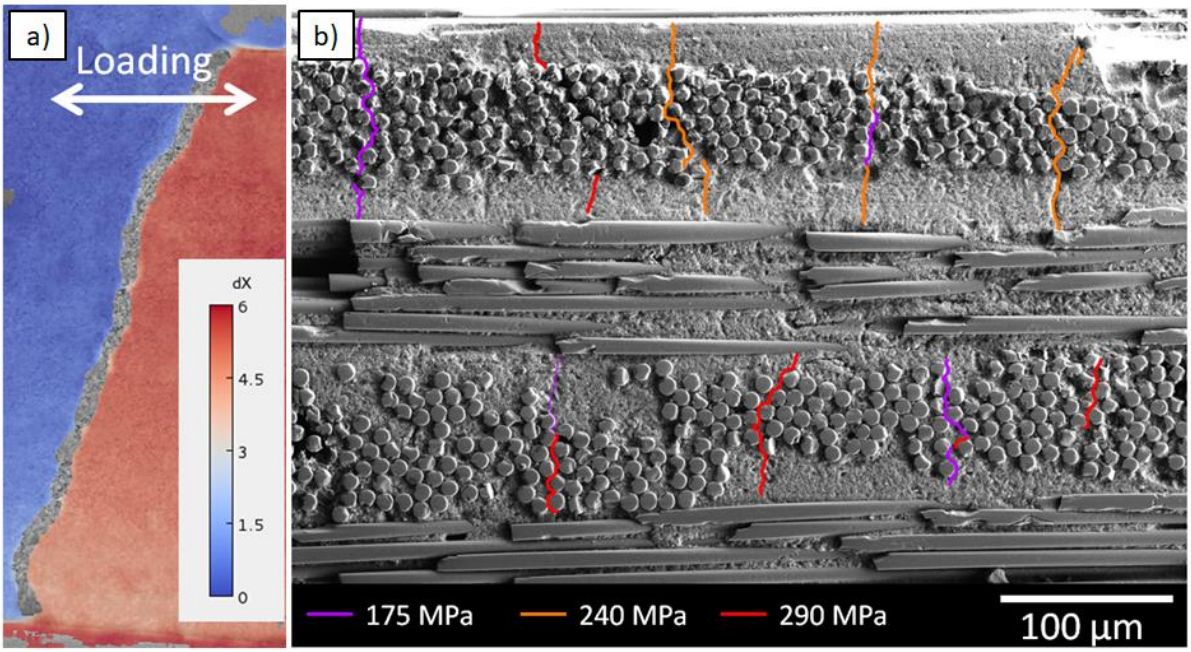

Figure 6 – SEM *in-situ* observation with DIC of a matrix crack (a) and crack development in the stretched part of a N610/Alumina composite sample subjected to 4 point bending.

In the part of the sample subjected to tension, cracks nucleation, openings and propagations were observed (Figure 6 (b)). Cracks appeared for stresses close to 150 MPa, which corresponds to the deviation from linearity observed on strain-stress curves. Cracks developed through transverse tows to form a periodic network. This type of multi-cracking is commonly observed on composites during tensile tests. A crack density gradient is also observed in the thickness of the sample: no more cracks being noted after the third ply. Moreover, no crack initiation or propagation was observed in the compressed part of the sample (Figure 7).

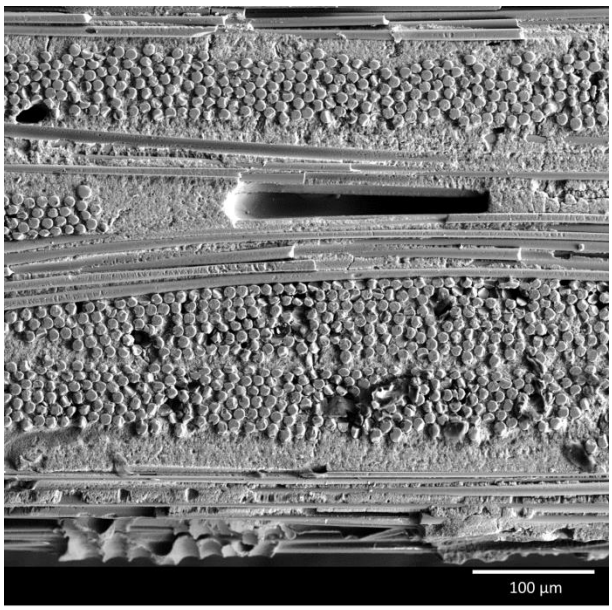

Figure 7 – SEM observation of the compressed part of a N610/Alumina composite subjected to four-point bending just before failure.

3.2. Effect of temperature on the elastic-damageable behaviour

First, the influence of the temperature on the mechanical behaviour was studied. Four specimens machined from the same plate were tested in tension at temperature ranging from 700 °C to 1000 °C and were compared to the reference tested at room temperature. Stress-strain curves are presented on Figure 8 (a). A drop of the rigidity was observed at 700 °C. Then the mechanical behaviour remained unchanged up to 900 °C and a notable viscous behaviour appeared at 1000 °C. In order to separate elastic and viscous strains, tests were performed at a displacement rate 100 times lower (5 µm.min^{-1}) on samples issued from the same plate. The two tests results are then compared (Figure 8 (b)). The 700 and 800 °C curves are superimposed so they are not represented. It indicates that there is no viscous behaviour at this temperature. At 900 and 1000 °C, the gap between the two tests increases with the stress, obviously revealing a viscous behaviour. Thus, for test duration longer than one hour, the viscous strain is no longer negligible above 800 °C and then should be taken into account for long-term applications.

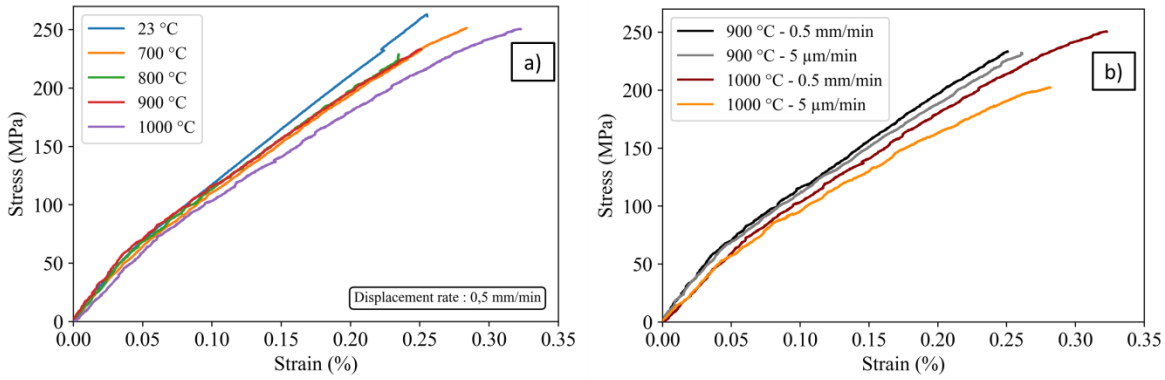

Figure 8 – Effect of temperature (a) and displacement rate (b) on the mechanical behaviour of a N610/Alumina composite.

Then, additional tests were conducted between 700 and 1000 °C to assess the mechanical properties. Table 2 summarises the measured Young's modulus, stress and strain at failure. The Young's modulus and the strength decrease at 700 °C, while the strain at failure remains constant. Ruggles-Wrenn *et al.* observed the same tendency on a N610/alumina composite processed through filament winding [30]. At 1100 °C, both Young's modulus and strength exhibited a 10% decrease while the failure strain remained approximately constant.

	Room Temperature (12 samples)	**700 °C (4 samples)**	**800 °C (4 samples)**	**900 °C (4 samples)**	**1000 °C (4 samples)**
Young modulus (GPa)	159 ± 7	139 ± 4	150 ± 4	134 ± 15	132 ± 9
Strain at the threshold (%)	0.029 ± 0.005	0.030 ± 0.007	0.034 ± 0.003	0.041 ± 0.007	0.045 ± 0.007
Stress at the threshold (MPa)	45 ± 6	45 ± 11	53 ± 5	54 ± 5	57 ± 7
E' (GPa)	95 ± 6	85 ± 2	85 ± 2	82 ± 5	77 ± 7
Strain at failure (%)	0.26 ± 0.02	0.26 ± 0.03	0.25 ± 0.02	0.25 ± 0.01	0.26 ± 0.02
Stress at failure (MPa)	257 ± 13	227 ± 10	224 ± 3	227 ± 10	225 ± 8

Table 2 – Mechanical properties in tension of a N610/Alumina composite up to 1000 °C.

The damage threshold, which is not well documented in the literature, was also measured. A small increase of the stress and the strain at the damage threshold is observed, while the temperature increases, especially at 800 °C and above. This phenomenon is not clearly explained but could be due to stresses relaxation within the matrix with the temperature. Also, the slope of the second linear part (E') tends to decrease with temperature due the reduction of the Young's modulus.

Cyclic loading tests (Figure 9) revealed a little effect of the matrix damage on the material behaviour beyond the damage threshold up to 900 °C: the mechanical behaviour is mainly controlled by the fibres. Nextel datasheet [31] indicates strength retention close to 100% at 900 °C. This is consistent with the small effect of the temperature on the tensile strength of the material.

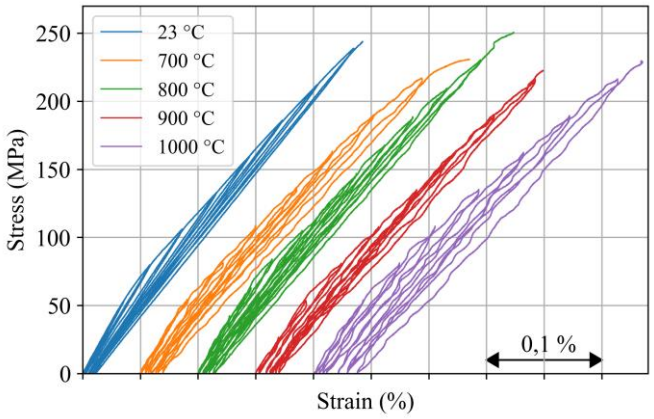

Figure 9 – Effect of temperature during cyclic loading tests on a N610/Alumina composite.

After these observations, some tests were performed at higher temperatures and more particularly at 1200 and 1300 °C. A dramatic change in the behaviour of the material (**Figure 10**) occurs: the strain at failure drastically increased to 13.5 ± 1.0% at 1200 °C and 15.5 ± 0.3% at 1300 °C. The Young's modulus dropped to 78 ± 7 GPa at 1200 °C and 62 ± 1 GPa at 1300 °C. The maximum stress also decreased significantly to 85 ± 3 MPa and 37.1 ± 0.5 MPa respectively. This change was also observed by Ruggles-Wrenn *et al.* [30]. At 1200 °C they measured a drastic decrease of the Young's modulus (-62%) and a strain at failure multiplied by 4.

This so called "superplastic" behaviour has already been observed on ceramics, especially on polycrystalline alumina. On pure alumina with small grains (0.5 µm), Xue and Chen [32] observed this behaviour at temperature as low as 1250 °C. At 1300 °C, they measured a compressive strain at failure beyond 60%. Ruano *et al.* reviewed numerous studies concerning the creep of polycrystalline alumina [33]. Most of the papers revealed a stress exponent close or equal to 2 associated to grain boundary sliding (GBS) accommodated by dislocation climb. Other studies mentioned stress exponents close to one. So superplastic behaviour of alumina is observed commonly associated with stress exponent lower than 2 [34]. Despite a stress exponent closer to 3 [35], N610 fibre is subjected to superplasticity at high temperature. The mechanisms are however different since Hay et al. showed important grain elongation in air (more than 50% of the total creep strain).

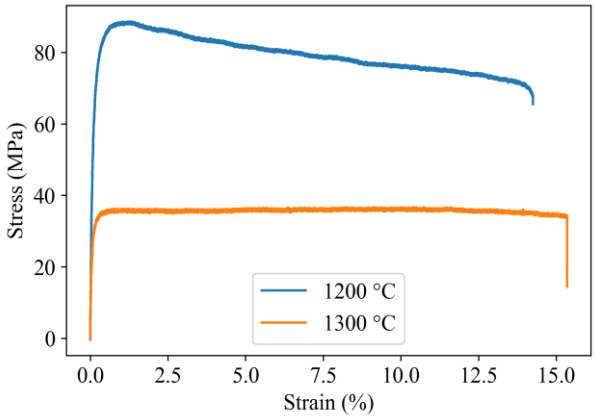

Figure 10 – Typical stress-strain tensile curve at 1200 and 1300 °C of a N610/alumina composite

A typical fracture surface observed below 1000 °C is illustrated in Figure 11. Some fibre extractions and delaminations can be observed. From 1200 °C and more particularly at 1300 °C, the fracture surface becomes planar.

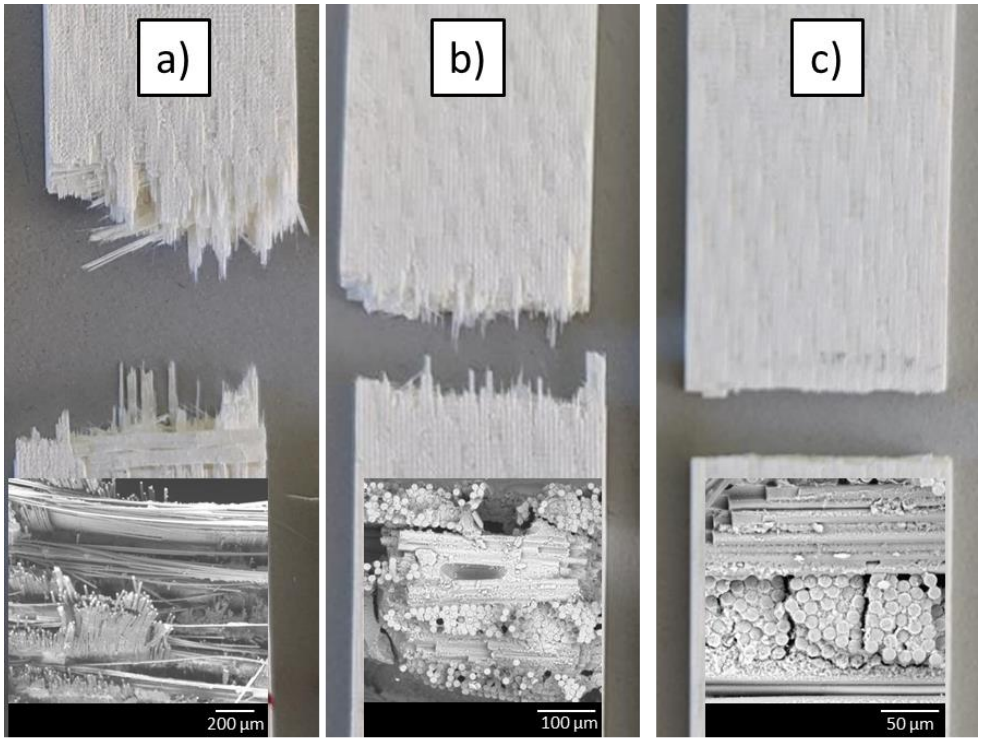

Figure 11 – Fracture surfaces of a N610/alumina composite after a tensile test below 1000 °C (a), at 1200 °C (b) and at 1300 °C (c).

The two last test temperatures are at least equal to the processing one so it was expected that the material would not be stable. Figure 12 illustrates the evolution of the thickness when an already sintered sample is subjected to a short term heat treatment in a dilatometer at 1200 °C. Shrinkage is observed at temperatures higher than 1050 °C. It is then clear that the one hour holding step conducted just before the tensile test results in a densification of the matrix and an increase of its cohesion with the fibres.

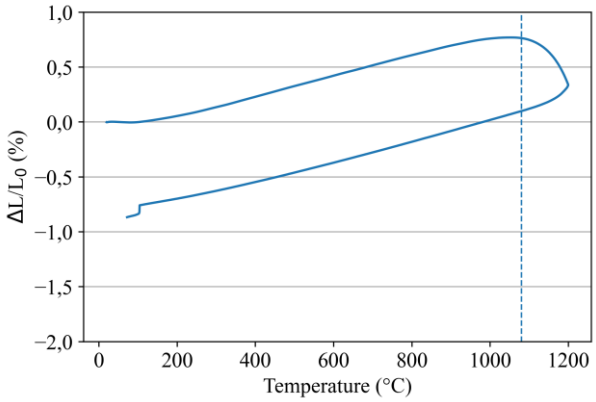

Figure 12 – Shrinkage in the thickness of a N610/Alumina composite during a representative treatment of the processing one.

The observation of a sample heat treated for 1h15 at 1300 °C confirmed the assumption of the sintering. The matrix exhibited less pores of bigger size (Figure 13).

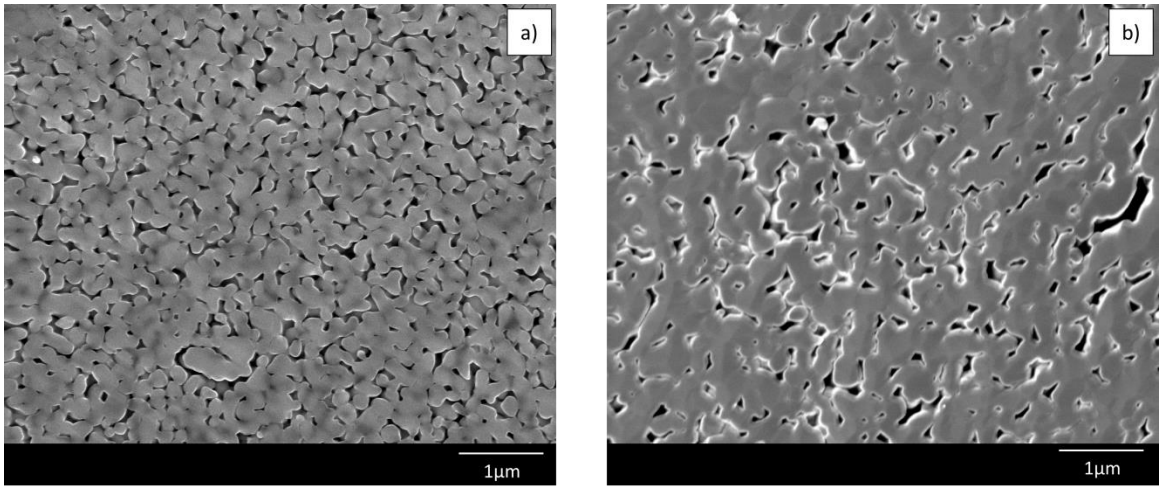

Figure 13 – Matrix observation of an as-processed (a) and a 1h15 - 1300 °C heat-treated N610/alumina composite (b)

Finally, these experiments allow us to propose a law to describe the evolution of the Young's modulus as a function of the temperature (Figure 14). The evolution was fitted by the empirical equation (1).

$$E = \frac{E_0}{1 + \exp\left(\frac{(T - T_{th})}{a}\right)} \quad (1)$$

The Young's modulus remained nearly constant from room temperature up to 600 °C and exhibited a slow decrease up to 1000 °C. A drastic drop is observed between 1000 °C and 1300 °C which is representative of the experiments.

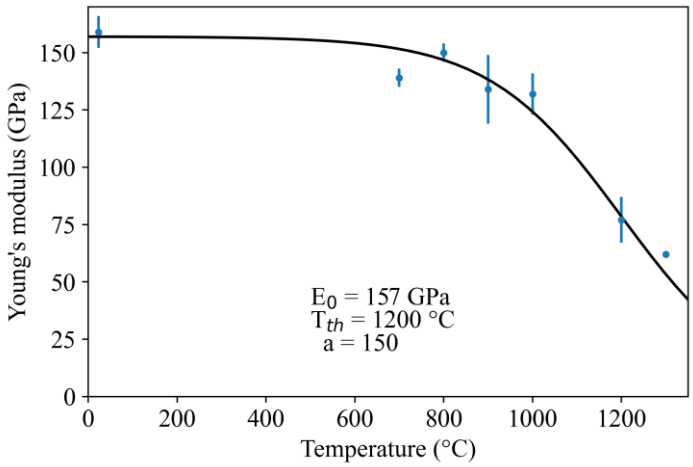

Figure 14 – Temperature dependence of the Young's modulus of a N610/Alumina composite.

Moreover, the effect of temperature on the bending behaviour was evaluated at 800 °C on 24 specimens. As for the tensile tests, a 10% decrease in both Young's modulus and stress at failure was observed at 800 °C. The results are presented in Table 3.

	Room Temperature (37 samples)	**800 °C (24 samples)**
Young's modulus (GPa)	111 ± 8	101 ± 9
Strain at failure (MPa)	0.26 ± 0.05	0.27 ± 0.04
Stress at failure (MPa)	286 ± 52	266 ± 48

Table 3 – Four-point bending properties of a N610/Alumina composite at room temperature and 800 °C.

Failure occurred in a similar way to what was observed at room temperature. The external ply subjected to tension broke first for a majority of the samples.

4. Conclusion

The influence of the temperature on the mechanical behaviour of a N610/Alumina composite was studied through tensile and four-point bending tests, from room temperature up to 1300 °C. Three temperature ranges characterize the mechanical behaviour. Up to about 800 °C the mechanical behaviour is not significantly affected by temperature: only a 10% decrease in Young's modulus and strength is observed. Between 800 °C and 1000 °C a viscous behaviour appeared, revealed by a tensile behaviour depending on the loading speed. From 900 °C, an increase in deformation was noted during slower tests. In this temperature range, the creep of the material must be considered for long-term applications. Above 1200 °C, i.e. the sintering temperature, a drastic decrease in stiffness and strains to failure of several percent were observed. The mechanical behaviour is close to a monolithic ceramic.

In four-point bending, a quasi-linear macroscopic response of the structure was observed. However, a dissymmetry of behaviour between tension and compression at the local scale was revealed by digital image correlation. A simple linear elastic behaviour was observed in the compression part. This was confirmed by four-point bending tests carried out under SEM, which did not reveal any damage in the compressed part. In contrast, damage was observed in the stretched part. The first cracks appear at a stress three times higher during bending tests which is allowed by load transfer between plies.

5. References

[1] R. C. Robinson and J. L. Smialek, 'SiC Recession Caused by SiO_2 Scale Volatility under Combustion Conditions: I, Experimental Results and Empirical Model', *Journal of the American Ceramic Society*, vol. 82, no. 7, pp. 1817–1825, Jul. 1999, doi: 10.1111/j.1151-2916.1999.tb02004.x.

[2] N. S. Jacobson, 'Corrosion of Silicon-Based Ceramics in Combustion Environments', *Journal of the American Ceramic Society*, vol. 76, no. 1, pp. 3–28, Jan. 1993, doi: 10.1111/j.1151-2916.1993.tb03684.x.

[3] S. Schmidt, S. Beyer, H. Knabe, H. Immich, R. Meistring, and A. Gessler, 'Advanced ceramic matrix composite materials for current and future propulsion technology applications', *Acta Astronautica*, vol. 55, no. 3–9, pp. 409–420, Aug. 2004, doi: 10.1016/j.actaastro.2004.05.052.

[4] F. W. Zok, 'Developments in Oxide Fiber Composites', *Journal of the American Ceramic Society*, vol. 89, no. 11, pp. 3309–3324, Nov. 2006, doi: 10.1111/j.1551-2916.2006.01342.x.

[5] D. Koch, K. Tushtev, and G. Grathwohl, 'Ceramic fiber composites: Experimental analysis and modeling of mechanical properties', *Composites Science and Technology*, vol. 68, no. 5, pp. 1165–1172, Apr. 2008, doi: 10.1016/j.compscitech.2007.06.029.

[6] K. A. Keller, G. Jefferson, and R. J. Kerans, 'Oxide-Oxide composites', in *Handbook of Ceramic Composites*, N. P. Bansal, Ed. Boston, MA: Springer US, 2005, pp. 377–421. doi: 10.1007/0-387-23986-3_16.

[7] F. F. Lange, W. C. Tu, and A. G. Evans, 'Processing of damage-tolerant, oxidation-resistant ceramic matrix composites by a precursor infiltration and pyrolysis method', *Materials Science and Engineering: A*, vol. 195, pp. 145–150, Jun. 1995, doi: 10.1016/0921-5093(94)06513-6.

[8] L. P. Zawada, 'Longitudinal and Transthickness Tensile Behavior of Several Oxide/Oxide Composites', in *Ceramic Engineering and Science Proceedings*, vol. 19, D. Bray, Ed. Hoboken, NJ, USA: John Wiley & Sons, Inc., 1988, pp. 327–339. doi: 10.1002/9780470294482.ch36.

[9] C. G. Levi, J. Y. Yang, B. J. Dalgleish, F. W. Zok, and A. G. Evans, 'Processing and Performance of an All-Oxide Ceramic Composite', *Journal of the American Ceramic Society*, vol. 81, no. 8, pp. 2077–2086, Jan. 2005, doi: 10.1111/j.1151-2916.1998.tb02590.x.

[10] B. N. Cox and F. W. Zok, 'Advances in ceramic composites reinforced by continuous fibers', *Current Opinion in Solid State and Materials Science*, vol. 1, no. 5, pp. 666–673, 1996.

[11] W. E. C. Pritzkow, R. S. M. Almeida, L. B. Mateus, K. Tushtev, and K. Rezwan, 'All-oxide ceramic matrix composites (OCMC) based on low cost 3M Nextel™ 610 fabrics', *Journal of the European Ceramic Society*, vol. 41, no. 5, pp. 3177–3187, May 2020, doi: 10.1016/j.jeurceramsoc.2020.05.070.

[12] C. Ben Ramdane *et al.*, 'Microstructure and mechanical behaviour of a Nextel™610/alumina weak matrix composite subjected to tensile and compressive loadings', *Journal of the European Ceramic Society*, vol. 37, no. 8, pp. 2919–2932, Jul. 2017, doi: https://doi.org/10.1016/j.jeurceramsoc.2017.02.042.

[13] D. M. Wilson and L. R. Visser, 'High performance oxide fibers for metal and ceramic composites', *Composites Part A: Applied Science and Manufacturing*, vol. 32, no. 8, pp. 1143–1153, Aug. 2001, doi: 10.1016/S1359-835X(00)00176-7.

[14] C. J. Armani, M. B. Ruggles-Wrenn, G. E. Fair, and R. S. Hay, 'Creep of Nextel ™ 610 Fiber at 1100°C in Air and in Steam', *International Journal of Applied Ceramic Technology*, vol. 10, no. 2, pp. 276–284, Mar. 2013, doi: 10.1111/j.1744-7402.2012.02831.x.

[15] H. M. Yun and C. Goldsby, 'Tensile Creep Behavior of Polycrystalline Alumina Fibers', NASA Technical Memorandum 106269, Jul. 1993.

[16] V. H. Hammond and D. M. Elzey, 'Comparing the creep response of alumina tows and single filaments', *Scripta Materialia*, vol. 46, no. 4, pp. 287–291, Feb. 2002, doi: 10.1016/S1359-6462(01)01240-4.

[17] S. Hackemann, F. Flucht, and W. Braue, 'Creep investigations of alumina-based all-oxide ceramic matrix composites', *Composites Part A: Applied Science and Manufacturing*, vol. 41, no. 12, pp. 1768–1776, Dec. 2010, doi: 10.1016/j.compositesa.2010.08.012.

[18] M. Ruggleswrenn and P. Laffey, 'Creep behavior in interlaminar shear of Nextel™720/alumina ceramic composite at elevated temperature in air and in steam☆', *Composites Science and Technology*, vol. 68, no. 10–11, pp. 2260–2266, Aug. 2008, doi: 10.1016/j.compscitech.2008.04.009.
[19] M. Ruggles-Wrenn and S. Hilburn, 'Creep in Interlaminar Shear of a Nextel ™ 720/aluminosilicate Composite at 1100°C in Air and in Steam', *International Journal of Applied Ceramic Technology*, vol. 12, no. 2, pp. 473–480, Mar. 2015, doi: 10.1111/ijac.12357.
[20] M. B. Ruggles-Wrenn, G. T. Siegert, and S. S. Baek, 'Creep behavior of Nextel™720/alumina ceramic composite with ±45° fiber orientation at 1200°C', *Composites Science and Technology*, vol. 68, no. 6, pp. 1588–1595, May 2008, doi: 10.1016/j.compscitech.2007.07.012.
[21] M. B. Ruggles-Wrenn, S. N. Minor, C. P. Przybyla, and E. L. Jones, 'Creep of a Nextel™720/alumina ceramic composite containing an array of small holes at 1200°C in air and in steam', *International Journal of Applied Ceramic Technology*, Aug. 2018, doi: 10.1111/ijac.13074.
[22] D. J. Buchanan, R. John, and L. P. Zawada, 'Off-axis creep behavior of oxide/oxide NextelTM720/AS-0', *Composites Science and Technology*, vol. 68, no. 6, pp. 1313–1320, May 2008, doi: 10.1016/j.compscitech.2007.12.013.
[23] L. P. Zawada, R. S. Hay, S. S. Lee, and J. Staehler, 'Characterization and High-Temperature Mechanical Behavior of an Oxide/Oxide Composite', *Journal of the American Ceramic Society*, vol. 86, no. 6, pp. 981–990, Jun. 2003.
[24] M. B. Ruggles-Wrenn, P. Koutsoukos, and S. S. Baek, 'Effects of environment on creep behavior of two oxide/oxide ceramic–matrix composites at 1200 °C', *Journal of Materials Science*, vol. 43, no. 20, pp. 6734–6746, Oct. 2008.
[25] Z. X. Wen, X. H. Zhang, X. W. Yue, C. J. Zhang, Y. L. Zhang, and Z. F. Yue, 'Monotonic tension behavior of 2D woven oxide/oxide ceramic matrix composites at ultra-high temperature', *Journal of the European Ceramic Society*, vol. 41, no. 6, pp. 3535–3546, Jun. 2021, doi: 10.1016/j.jeurceramsoc.2021.01.001.
[26] R. Jiang, L. Yang, H. Liu, X. Sun, and H. Cheng, 'High-temperature mechanical properties of Nextel TM 610 fiber reinforced silica matrix composites', *Ceramics International*, vol. 44, no. 13, pp. 15356–15361, Sep. 2018, doi: 10.1016/j.ceramint.2018.05.185.
[27] N. Guel *et al.*, 'Data Merging of AE Sensors with Different Frequency Resolution for the Detection and Identification of Damage in Oxide-Based Ceramic Matrix Composites', *Materials*, vol. 13, no. 20, p. 4691, Oct. 2020.
[28] A. Gasser, P. Ladeveze, and M. Poss, 'Damage-mechanisms-of-a-woven-SiCSiC-composite-Modelling-and-identificationComposites-Science-and-Technology.pdf', *Composites Science and Technology*, vol. 56, pp. 779–784, 1996.
[29] G. Camus, 'Modelling of the mechanical behavior and damage processes of fibrous ceramic matrix composites: application to a 2-D SiC/SiC', *International Journal of Solids and Structures*, vol. 37, pp. 919–942, 2000.
[30] M. B. Ruggles-Wrenn, S. S. Musil, S. Mall, and K. A. Keller, 'Creep behavior of NextelTM610/Monazite/Alumina composite at elevated temperatures', *Composites Science and Technology*, vol. 66, no. 13, pp. 2089–2099, Oct. 2006, doi: 10.1016/j.compscitech.2005.12.026.
[31] 'Technical Reference Guide'. 3M Nextel Ceramic Fibers and Textiles, 2018. Accessed: Jun. 07, 2021. [Online]. Available: http://multimedia.3m.com/mws/media/1327055O/3m-nextel-technical-reference-guide.pdf.
[32] L. A. Xue and I.-W. Chen, 'Deformation and Grain Growth of Low-Temperature-Sintered High-Purity Alumina', *Journal of the American Ceramic Society*, vol. 73, no. 11, pp. 3518–3521, Nov. 1990, doi: 10.1111/j.1151-2916.1990.tb06489.x.
[33] O. A. Ruano, J. Wadsworth, and O. D. Sherby, 'Deformation of fine-grained alumina by grain boundary sliding accommodated by slip', *Acta Materialia*, vol. 51, no. 12, pp. 3617–3634, Jul. 2003, doi: 10.1016/S1359-6454(03)00180-0.

[34] Z.-R. Lin, A. H. Chokshi, and T. G. Langdon, 'An investigation of grain boundary sliding in superplasticity at high elongations', *Journal of Materials Science*, vol. 23, no. 8, pp. 2712–2722, Aug. 1988, doi: 10.1007/BF00547441.

[35] R. S. Hay, C. J. Armani, M. B. Ruggles-Wrenn, and G. E. Fair, 'Creep mechanisms and microstructure evolution of Nextel™ 610 fiber in air and steam', *Journal of the European Ceramic Society*, vol. 34, no. 10, pp. 2413–2426, Sep. 2014, doi: 10.1016/j.jeurceramsoc.2014.01.032.